

Loss of 12 Starlink Satellites Due to Pre-conditioning of Intense Space Weather Activity Surrounding the Extreme Geomagnetic Storm of 10 May 2024

Ayisha M Ashruf¹, Ankush Bhaskar¹, C Vineeth¹, Tarun Kumar Pant¹, and Ashna V M²

¹Space Physics Laboratory, Vikram Sarabhai Space Centre, Thiruvananthapuram, Kerala, 695022, India
²Department of Physics, Providence Women's College, University of Calicut, Malaparamba, Kerala, India

Key Points:

- Sudden increase in the orbital decay of Starlink satellites due to pre-conditioned space weather
- Effect limited to altitudes above 320 km, could be due to enhanced O/N_2
- Further, a sharp decline in altitude occurs 3 days post main phase of storm

arXiv:2410.16254v1 [physics.space-ph] 21 Oct 2024

Corresponding author: Ayisha M. Ashruf, ayisha@vssc.gov.in, ayishamashruf@gmail.com

Abstract

This study investigates the orbital decay and subsequent reentries of 12 Starlink satellites from 16 April to 15 May 2024. By examining Two-Line Element data, we observed a significant increase in orbital decay following the geomagnetic storm on 10 May 2024, consistent with expectations of increased thermospheric density. An unexpected increase in decay rates for 10 satellites was identified around 25 April 2024, while two lower-altitude satellites remained unaffected. Detailed analysis revealed that this enhanced decay rate prior to the storm was influenced by a spike in the O/N₂ ratio and an increase in Extreme Ultra Violet (EUV) flux. Moreover, most of the satellites exhibited sharp decay during the early recovery phase of the geomagnetic storm. Based on the positions and local times of changes in decay rates, it is likely that the satellites were affected by various processes during elevated space weather activity, such as enhanced EUV flux, Joule heating, particle precipitation, and the equatorial neutral anomaly. This study highlights the complex role of preconditioning due to enhanced EUV flux and extreme space weather activity in the orbital dynamics of Low-Earth Orbit (LEO) satellites.

Plain Language Summary

This study examines how preconditioned space weather, and an extreme geomagnetic storm on 10 May 2024, affected the orbits of 12 Starlink satellites. Notably, 10 of these satellites experienced increased drag even before the storm, around 25 April 2024, likely due to a rise in the global O/N₂ ratio from increased solar EUV radiation. After the storm, the satellites encountered even greater drag force, resulting in rapid orbital decay. This increase in drag was caused by increased atmospheric density linked to the storm and enhanced EUV radiation. These findings underscore the need to better understand the impact of preconditioned space weather and extreme events on the thermosphere, especially as more satellites are being launched into LEO.

1 Introduction

Atmospheric drag is the primary force driving the orbital decay of satellites, and it depends on several factors: the local atmospheric density, the satellite's cross-sectional area, its velocity, and the drag coefficient. The drag coefficient quantifies the interaction between the spacecraft's surface and the impinging atmospheric molecules within the free-molecular flow regime (Doornbos & Klinkrad, 2006). The most significant variable affecting drag is atmospheric density, which is largely driven by solar activity. Space weather events, such as geomagnetic storms and coronal mass ejections (CMEs), can cause abrupt increases in atmospheric density. When charged particles from CMEs reach Earth, they interact with the magnetosphere, generating increased currents in the magnetosphere-ionosphere system and causing Joule heating, particle precipitation, and expansion in the thermosphere (Sutton et al., 2009). This can lead to a substantial increase in atmospheric density at satellite altitudes, particularly during geomagnetic storms, where the total mass density can rise by more than an order of magnitude (Forbes et al., 2005). For satellites in LEO, this increased density results in greater drag forces, which can alter satellite trajectories, reduce their operational lifespans, and necessitate more frequent orbit maneuvers (Zesta & Oliveira, 2019). Moreover, (Oliveira et al., 2020) has quantified the possible impact of the historic extreme geomagnetic storms on satellite drag, showing the possibility of severe orbital decay. Disruptions from space weather events thus have significant impacts on satellite operations, affecting everything from satellite navigation to weather forecasting.

Space weather is mainly controlled by solar activity. We are in the ascending phase of solar cycle 25 and possibly near the solar maxima presently (Espuña Fontcuberta et al., 2023). Therefore, the sun has shown elevated activity, manifesting frequent geomagnetic disturbances, with aurorae being seen at low-latitudes (Vichare et al., 2024). Recently,

AR3664, an active region on the Sun, appeared on the south-eastern limb of the visible solar disk on 1 May 2024. It rapidly intensified between 3 and 6 May, leading to multiple X-class solar flares and CMEs directed toward Earth. This resulted in one of the most intense geomagnetic storms of the past two decades, which hit the Earth on 10 May 2024 (Hayakawa et al., 2024; Lazzús & Salfate, 2024). The impact of the storm resulted in global visibility of aurorae, even at mid-latitudes, and had severely affected the ionosphere-thermosphere system, uplifting the ionosphere to higher altitudes (Karan et al., 2024; Thampi et al., 2024; Kwak et al., 2024). Furthermore, the storm had impacted the Earth’s radiation belts, resulting in a strong Forbush decrease in cosmic rays reaching the Earth (Pierrard et al., 2024; Mavromichalaki et al., 2024). The impact of the storm on satellite drag has also been reported in Parker & Linares (2024).

Based on data from the Space-Track website (<https://www.space-track.org>), 54 orbiting bodies reentered Earth’s atmosphere from 1 to 15 May 2024. Among them, 12 were Starlink satellites (Table 1). Out of the 54 objects, 36 were in high-inclination to near-polar orbits, while the remaining 14, including the Starlink satellites, had inclinations of less than 53° . It was noted that the Starlink satellites that were not affected were at higher altitudes above 500 km, while the 12 satellites included in this study were situated at altitudes between 300 and 400 km. To evaluate the impact of this extreme geomagnetic storm and prior space weather conditions, we investigate the orbital decay experienced by these 12 Starlink satellites using available Two-Line Element set data, geomagnetic, and interplanetary data from 16 April 2024 to 15 May 2024. This study provides a unique opportunity to assess the impact of the extreme storm on LEO satellites, as no such severe storm has been experienced by satellites in the last two decades.

2 Data and Methodology

To examine the orbital decay of the satellites under consideration the Two-Line Element sets (TLEs) are used. TLEs summarize the orbital parameters into a maximum of 69 alphanumeric characters. A detailed description of the TLE format can be found in (Vallado & Cefola, 2012). TLE data from 16 April 2024 to 15 May 2024, for the objects listed in Table 1 were obtained from the Space-Track website. The semi-major axis ‘a’ of the orbit of each satellite at a given epoch is obtained from mean motion using the following equation,

$$a = \left(\frac{GM}{\left(\frac{2\pi n}{86400}\right)^2} \right)^{\frac{1}{3}} \quad (1)$$

where M is the mass of the Earth, G is the universal gravitational constant, and n is the mean motion in revolutions per day, as provided in the TLE dataset.

It is known that atmospheric temperature, composition, and density are strongly influenced by space weather effects, especially the change in solar EUV radiation and CMEs (Doornbos & Klinkrad, 2006). To examine the connection between EUV radiation and the observed decay, EUV flux data from the Solar Dynamics Observatory is analyzed. This data is crucial for understanding the changes associated with variations in solar output that can result in the variability of the ionosphere-thermosphere region.

The orbital decays are then plotted against the Dst indices, peak O/N₂ ratios, and EUV flux. The Extreme Ultraviolet Variability Experiment (EVE) onboard NASA’s Solar Dynamics Observatory (SDO) measures the solar EUV irradiance from 0.1 to 105 nm (Woods et al., 2012). The absorption of EUV (10–120 nm) and UV (120–200 nm) radiation accounts for roughly 80% of the energy entering the thermosphere. This process raises the temperature of the thermosphere, leading to its upwelling and downwelling as the EUV irradiance increases or decreases with the movement of active regions across the solar

disk (Vourlidis & Bruinsma, 2018). Since EUV radiation is the primary energy input at LEO altitudes, affecting the geospace environment and satellites, the EUV flux data from SDO (<https://sdo.gsfc.nasa.gov/data/>) between 16 April 2024 and 15 May 2024 is also examined in this study.

The interplanetary conditions are monitored using the ACE and WIND satellites, which observe upstream solar wind, while geomagnetic activity is tracked by ground-based magnetometer observatories worldwide. Data on solar wind and interplanetary magnetic fields are obtained from CDAWEB (<https://cdaweb.gsfc.nasa.gov/>), and the Dst index and auroral indices are sourced from the World Data Center in Kyoto (<https://wdc.kugi.kyoto-u.ac.jp/>).

The ratio of O to N₂ number densities (O/N₂) at various altitudes is an important parameter used to understand changes in thermospheric neutral composition and their impact on the ionosphere during varying geomagnetic conditions (Yu et al., 2023). The oxygen and nitrogen number densities are obtained using the NRLMSIS 2.0 empirical atmospheric model (Emmert et al., 2021).

3 Observations

3.1 Solar and Interplanetary Conditions

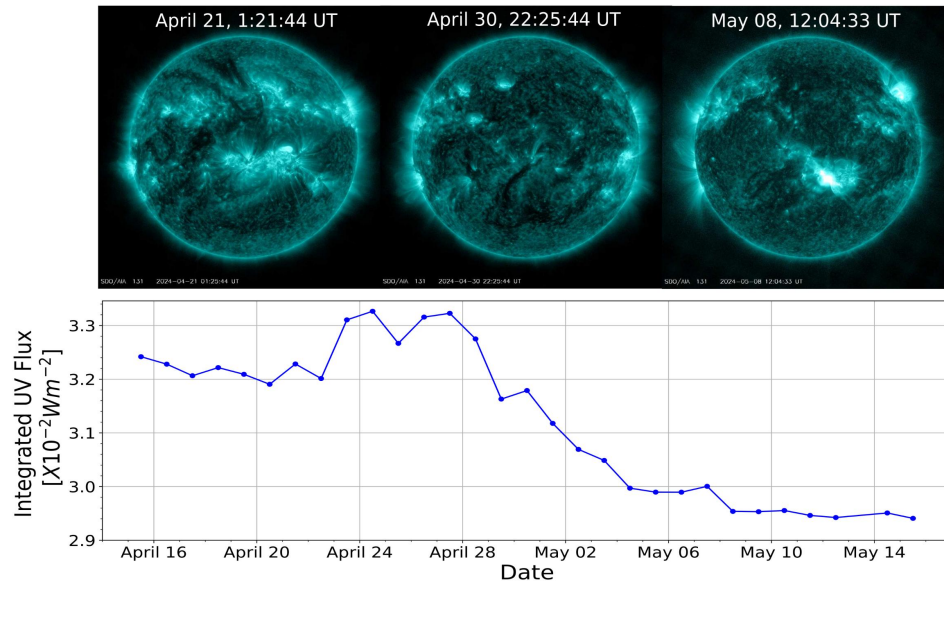


Figure 1. (top panel) Solar UV emission in 131 nm wavelength (bottom panel) Integrated UV emission over disk during 16 April 2024 and 15 May 2024, as observed by SDO.

The increased magnetic activity of the Sun led to the formation of numerous active regions and higher UV and EUV emissions from the solar disk. Figure 1 displays snapshots of the solar disk captured by the SDO in UV emissions at 131 nm. It is evident that the solar disk exhibited multiple bright emission regions around 21 April, with decreased emissions observed around 30 April, and then a subsequent increase in emissions by 8 May 2024. The flaring of active region AR3664 on the Sun is seen in the rightmost image of the disk. The temporal variation of integrated UV flux is illustrated in the bottom panel, indicating a high integrated flux between 21 April and 28 April 2024. Although UV fluxes decreased after 8

May, the geomagnetic activity remained high due to the impact of multiple ICMEs. Figure 2 depicts the solar wind, interplanetary, and geomagnetic parameters during the specified interval. The strongest perturbations in most of the solar wind parameters were seen on 10 May 2024. The IMF strength exceeded 60 nT, solar wind speed surpassed 800 km/s, and density and solar wind dynamic pressure peaked around 60 cm^{-3} and 60 nPa respectively, and the magnetopause moved inward below $6 R_E$. Before this solar storm, there were small fluctuations in the interplanetary magnetic field and solar wind parameters. The Sym-H index did not show a significant decrease, indicating relatively low geomagnetic activity prior to the intense storm. We will revisit the IP conditions in detail in the observations section.

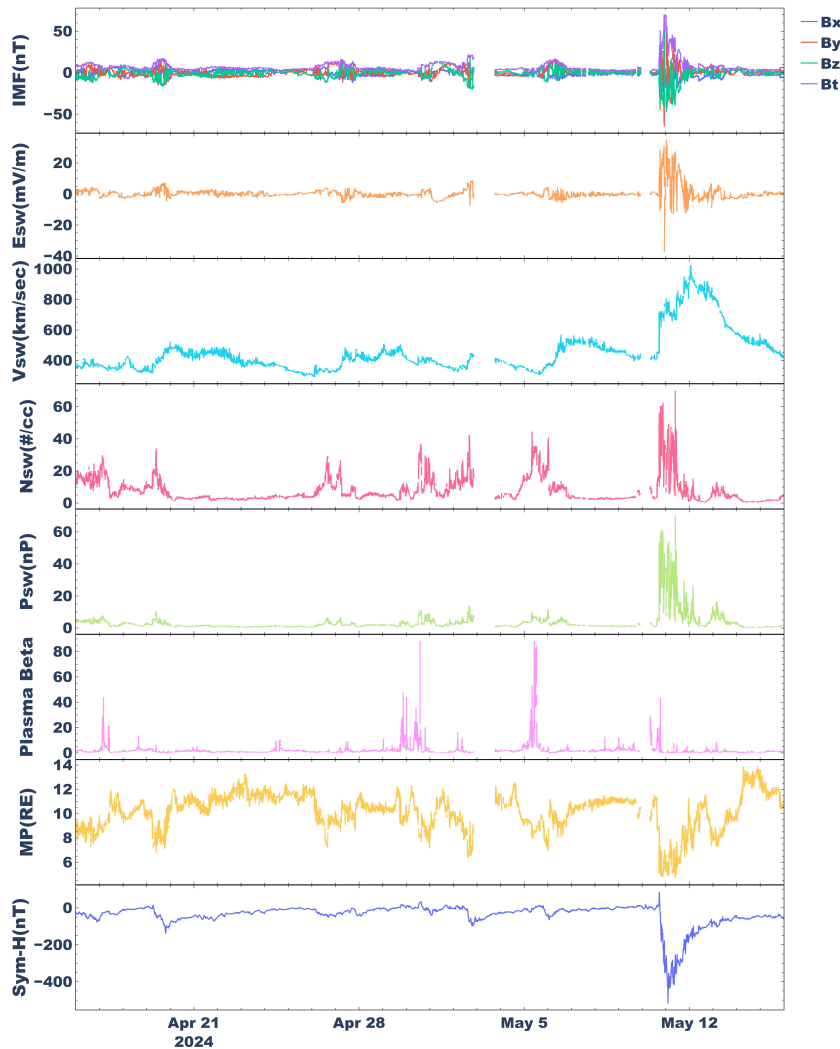


Figure 2. Interplanetary magnetic field parameters and solar wind velocity between 16 April 2024 and 15 May 2024

3.2 Impact on Starlink Satellite Orbits

Figure 3a depicts the orbital decay profiles of the 12 Starlink satellites alongside the Dst indices from 16 April 2024 to 15 May 2024. As expected, the satellites exhibited sharp orbital decay following the geomagnetic storm of 10 May 2024, primarily due to the increase in thermospheric density caused by the storm. However, an unexpected rise in orbital decay was observed in 10 of these satellites around 25 April 2024, while 2 satellites at lower altitudes of 320 km did not show this effect. This was intriguing since such a sharp change in decay occurred during a geomagnetically quiet time. The values of rates of decay of these objects during distinct time intervals are listed in Table 1.

A few interesting things can be noted from Figure 3a. Satellite 57649, initially at an altitude of approximately 400 km, experienced a decay rate of 0.7 km per day until around 26 April 2024. After this, the decay rate increased to about 8.1 km per day, and finally, there was a sharp rise to 45.3 km per day from 6 May 2024, leading to its reentry into the atmosphere. It must be noted that the second change in slope for this object occurred before the storm, unlike the other 11 satellites, where the second change in the rate of decay occurred after the storm's commencement.

Satellites 44951 and 44928, both starting at an altitude of 320 km on 16 April 2024, experienced constant decay rates of 2.2 km/day and 2 km/day, respectively. However, their decay rates sharply increased to 49.5 km/day and 57.4 km/day from 14 May 2024, leading to their reentry. The remaining objects exhibit a similar trend of sharp decay occurring 3 days after the main phase, except for object 48384, where the sharp decay aligns with the main phase of the storm.

Table 1. Satellites, inclination and slopes across three regions: inc - inclination, m1 - slope in region 1, m2 - slope in region 2, m3 - slope in region 3

NORAD ID	inc($^{\circ}$)	m1 (km/day)	m2 (km/day)	m3 (km/day)
57649	42.98	-0.73	-8.13	-45.37
48384	53.04	-1.08	-5.00	-56.40
48599	53.04	-0.14	-5.58	-61.47
48324	53.04	-1.47	-5.49	-71.41
44951	52.99	-2.27	-	-49.51
54001	53.21	-0.07	-5.32	-46.82
48430	53.07	-0.14	-5.42	-75.95
47915	53.02	-0.10	-5.53	-58.22
44928	53.04	-2.05	-	-57.44
48579	53.04	0.42	-5.35	-46.62
48308	53.03	-0.06	-5.71	-49.65
47741	53.02	-0.02	-5.57	-51.16

The sudden increase in altitude decay following the geomagnetic storm is expected. However, to understand the enhanced orbital decay observed around April 25, 2024, we analyze the peak O/N₂ ratios at 350 km, as well as the EUV flux data from the SDO. Figure 4 shows the TLE-derived altitude profiles of 12 satellites, plotted alongside the global peak ratios of atomic oxygen to molecular nitrogen number density at 350 km. A closer look at the figure shows that there is a sudden spike in the global peak of O/N₂ ratio on 25 April 2024.

The EUV irradiance data shown in Figure 3b indicates an enhancement between 24 April and 28 April 2024. This enhancement coincides with an increased rate of decay of the 10 objects during this period.

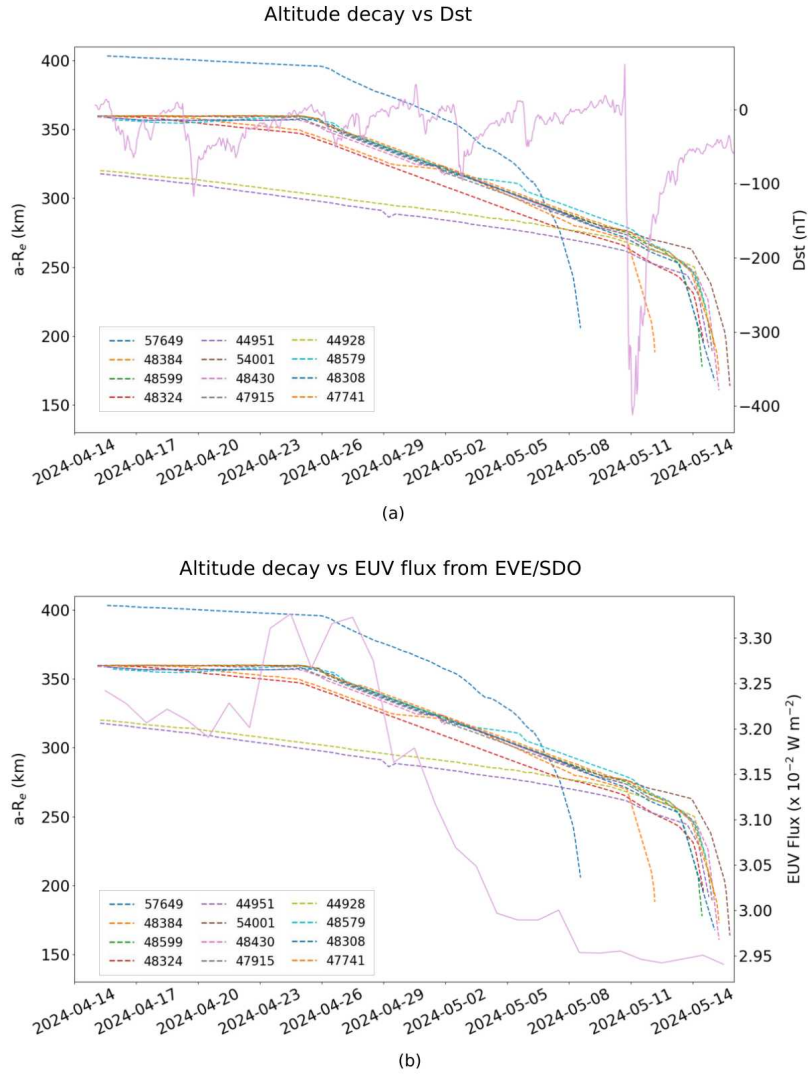


Figure 3. TLE derived altitude decay profile of the 12 Starlink satellites plotted against (a) Dst values between 16 April 2024 to 15 May 2024 (b) EUV flux data from EVE/SDO.

The O/N_2 ratio is a critical parameter for evaluating the impact of the space weather events on the thermosphere heating and cooling. Examining the O/N_2 ratio maps from various epochs before and during the storm (Figure 5), a significant decrease in the O/N_2 ratio is observed during the storm. However, at 04:00 UT on 19 April and 02 May 2024, when geomagnetic activity was low, the O/N_2 ratios were nearly twice as high as those observed during the storm. Additionally, on 25 April 2024 at 20:00 UT, the O/N_2 ratio peaks, with the highest values concentrated in the southern hemisphere.

Figure 7 represents the variations of hourly OMNI data (King & Papitashvili, 2020). The variations in the disturbance storm time (Dst) index clearly show the main phase and recovery phase intervals, which are marked by dotted vertical lines. In panel ‘a’ of figure 7, the magnitude of the interplanetary magnetic field (IMF) and its components B_x , B_y , and north-south component B_z are presented. The IMF magnitude sharply increased from

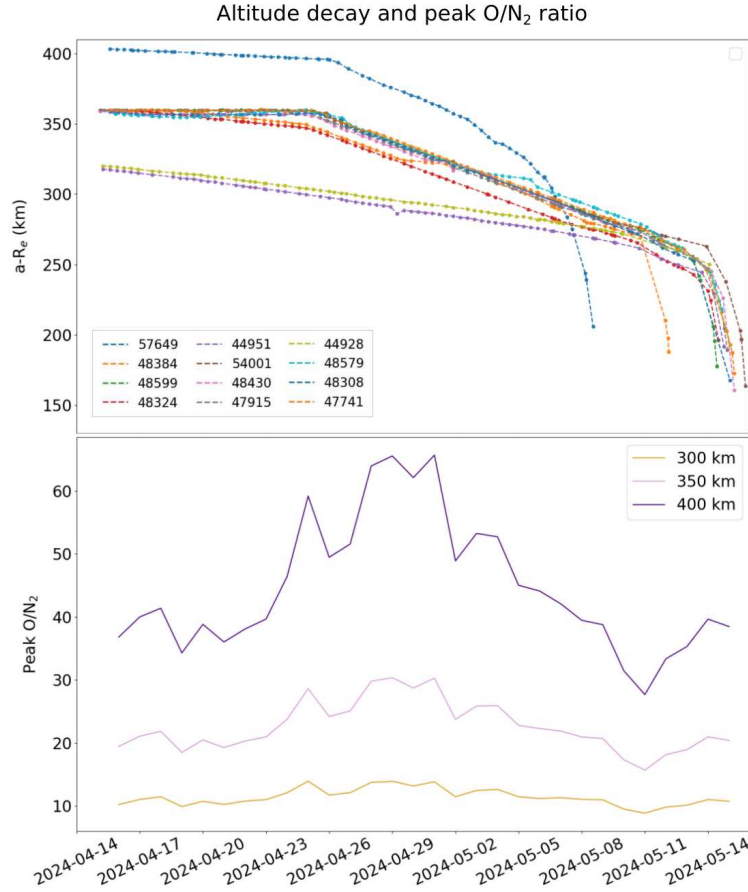


Figure 4. TLE derived altitude decay profile of the 12 Starlink satellites plotted against global peak O/N₂ ratios at 300 km, 350 km and 400 km altitudes between 16 April 2024 to 15 May 2024

1.6 nT at 05:30 UT to a maximum of 68.9 nT at 23:30 UT on 10 May 2024. It remained significantly elevated throughout 11 May, not decreasing below 10 nT until the early hours of 12 May. Throughout most of this period, the B_z component remained primarily oriented southward (negative), reaching values as low as -35 nT at 21:00 UT on 10 May, and at 00:00 UT and 09:00 UT on 11 May. The persistently southward IMF component drove continuous magnetic reconnection at the dayside magnetopause, enhancing plasma convection within the inner magnetosphere and polar cap. This process eventually triggered reconnection in the magnetotail, linked to plasma injections. From panel ‘b’ of figure 7, it can be seen that the solar wind speed increased continuously from 398 km/s on 10 May 2024, at 01:30 UT to a maximum value of 1006 km/s on 12 May 2024. When the Dst and the peak IMF field strength reached their minimum, the solar wind speed was 738 km/s on 11 May at 02:30 UT. The solar wind speed then slowly started decaying and reached a minimum of 428 km/s on 15 May 15 at 23:30 UT. The solar wind density started increasing until it reached a maximum value of 48.1 cm⁻³ on 10 May 2024, at 20:30 UT.

Regarding the AE and Dst indices, whenever IMF-B_z turns southward, activity in Dst and AE indices peaks up due to the magnetic reconnection between the southward-directed IMF-B_z and geomagnetic field lines and strong substorm activity. This allows solar wind particles to enter the coupled magnetosphere-ionosphere environment, inducing geomagnetic activity as observed by the sharp changes in the indices (Poudel et al., 2019). The main

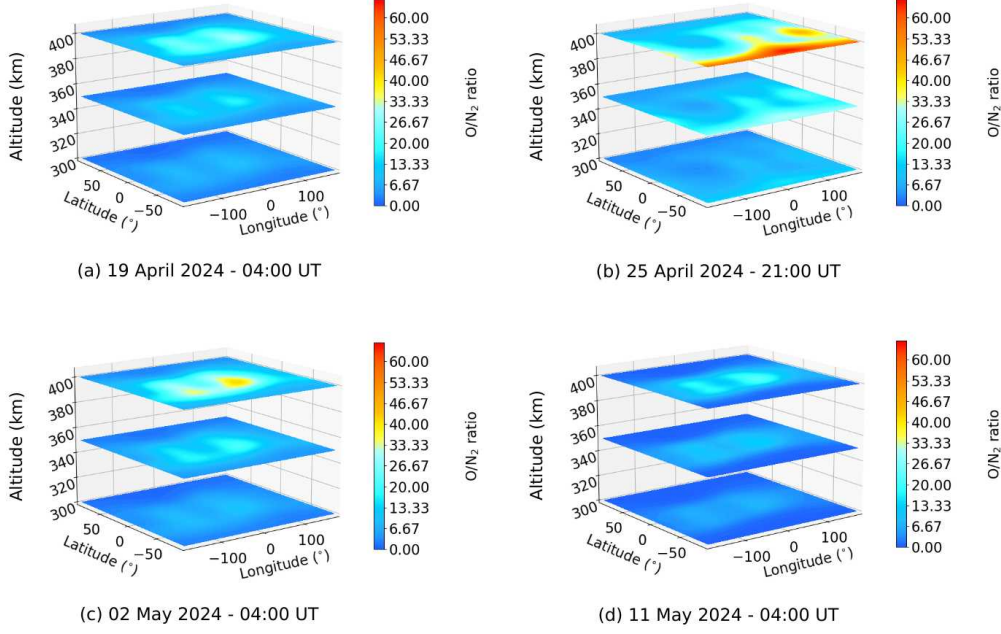


Figure 5. O/N_2 ratio maps at 300 km, 350 km, and 400 altitudes for (a) 19 April 2024 (b) 25 April 2024 (c) 02 May 2024, and (d) 11 May 2024

phase here which lasts for 9 hours is characterized by very strong intensity as observed in the Dst index having -461 nT minimum. Panels ‘e’, ‘f’ and ‘g’ represent the various energy estimates of the intense storm that occurred on 10 May 2024. The ring current injection rate U_{RC} , joule heating of the magnetosphere U_J , and auroral precipitation U_A are the major forms of dissipation of the energy in the magnetosphere. The Dst index is influenced by magnetopause currents; therefore, in this study, we have corrected the Dst values using solar wind ram pressure to remove this contamination (Burton et al., 1975; Vichare et al., 2005).

$$Dst^* = Dst - b \times p^{1/2} + C \quad (2)$$

where, P is solar wind dynamic pressure, and the coefficients are set to $b = 7.26$ nT and $c = 11$ nT (Wang et al., 2003; O’Brien & McPherron, 2000). The total magnetospheric energy consumption rate can be determined by using quantitative estimation given by (Akasofu, 1981). The total energy contains a major contribution from three components - U_J , U_A and U_{RC} (Akasofu, 1981; Vichare et al., 2005) which are defined by the following equations.

$$U_T = U_J + U_A + U_{RC} \quad (3)$$

$$U_J = 2 \times 10^8 AE \quad (4)$$

$$U_A = 1 \times 10^8 AE \quad (5)$$

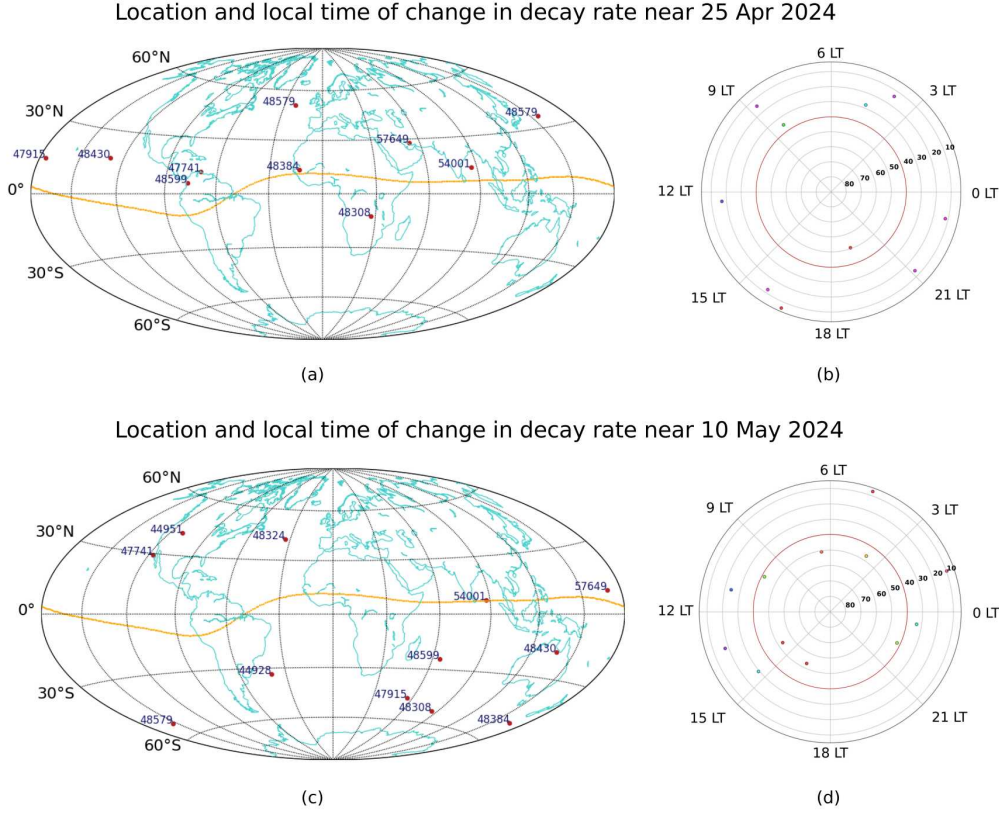


Figure 6. (a) Coordinates of change in the rate of decay near 25 April 2024 (b) and corresponding local time vs latitude map (c) coordinates of change in the rate of decay near 10 May 2024 (d) and corresponding local time vs latitude map.

$$U_{RC} = -4 \times 10^{13} \left(\frac{d(Dst^*)}{dt} + \frac{Dst^*}{\tau} \right) \quad (6)$$

where, Dst^* is the pressure corrected disturbance storm time index (in nT) and τ is the decay time constant as 8 hours for intense geomagnetic storms (Yokoyama & Kamide, 1997).

Panel ‘e’ shows that maximum value of U_J and U_A are 393 GW and 196 GW on 11 May 2024 at 13:30 UT respectively. Panel ‘f’ shows a minimum value of U_{RC} -1109 on 10 May 2024 at 18:30 UT and a maximum value is 1333 on 11 May at 09:30 UT. Panel ‘g’ shows the minimum value of U_T -778 GW on 10 May at 18:30 UT and a maximum value of 1919 GW on 11 May at 09:30 UT. On 11 May 2024, at 02:30 UT when Dst reached its minimum value, the U_J , U_A , U_{RC} , U_T were 202 GW, 101 GW, 357 GW, 661 GW respectively. The AE index was 1014 nT. The energy estimates show that a huge amount of energy was deposited into the magnetosphere-ionosphere system, which resulted in enhanced thermospheric heating during this intense storm.

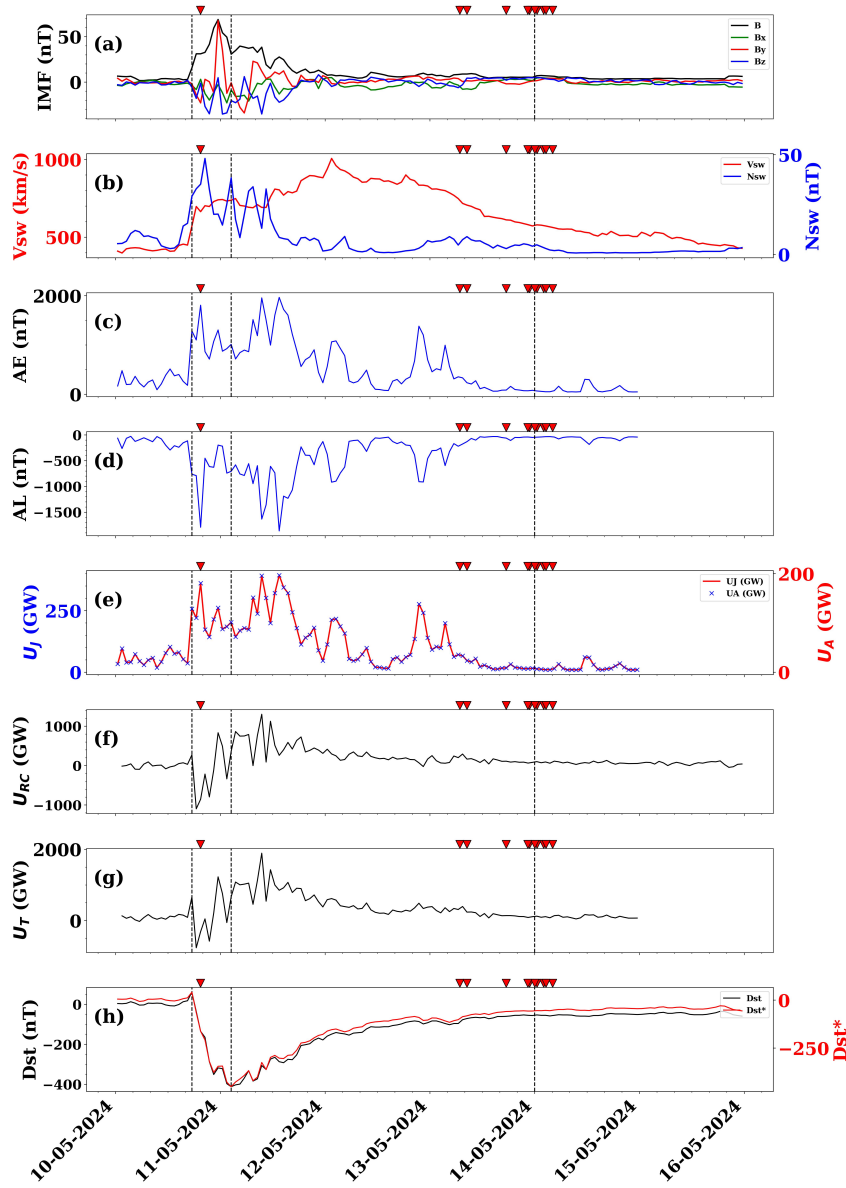


Figure 7. Various geophysical parameters associated with the geomagnetic storm. The three vertical dashed lines represent key phases of the storm: the leftmost line marks the onset of the storm and the beginning of the main phase, the second line indicates the minimum Dst index and the end of the main phase, and the rightmost line signifies the start of the recovery phase where Dst variations stabilize. Triangular symbols correspond to observations of decayed Starlink satellites, based on TLE data, reflecting the storm’s impact on satellite trajectories.

4 Discussion

The observed orbital decay and subsequent reentries of 12 Starlink satellites during the geomagnetic storm on 10 May 2024, offer valuable insights into the impact of space weather on satellites in LEO. The sharp increases in orbital decay following the storm were expected. However, the unexpected rise in the rate of orbital decay experienced by 10 of the satellites around 25 April 2024 required further analysis to understand the underlying mechanisms. Joule heating, caused by resistive heating from a current flowing through an electric field, occurs in the thermosphere due to the dissipation of auroral electrojet currents. It is the second most significant energy sink following the ring current (Baumjohann & Kamide, 1984; Chun et al., 2002). Joule heating is primarily concentrated at E-region altitudes, where Pedersen conductivity is highest (Huang et al., 2012). Figure 7 depicts the interval centered around the geomagnetic storm showing incident energy in the ionosphere due to Joule heating (U_J) and auroral particle precipitation (U_A). The figure shows a significant energy input to the ionosphere during the storm. As a result, density perturbations at LEO altitudes are mainly driven by the upwelling of neutral particles and the expansion of the thermosphere due to heating pressure from below (Lu et al., 2016; Billett et al., 2024). This thermospheric expansion increases atmospheric density at LEO altitudes, resulting in higher drag forces on satellites, with the effect being most pronounced at mid to high latitudes. Satellite 47915, for instance, showed an increase in decay above 50° N latitude around 25 April 2024, likely due to Joule heating of the thermosphere.

The equatorial anomaly refers to the anomalous latitudinal distribution observed in both the ionized and neutral components of the atmosphere. Specifically, the equatorial ionization anomaly (EIA) describes this irregular distribution in ions. The electron crest region exerts drag on the neutrals, leading to an increase in their density in the surrounding area (Oigawa et al., 2021), which causes the neutral anomaly. The neutral anomaly becomes more pronounced at higher solar flux levels (Liu et al., 2007) and figure 3b shows significant enhancement in EUV flux over this time period. Figure 6 depicts the locations and local time of the first change in the decay rates of the 10 satellites. Satellites 48599, 54001, 48430, 48579, and 48308 appear to have been affected by this phenomenon when passing through low latitudes (Figure 6).

A notable observation is that the two satellites that did not show a change in their orbital decay rates around 25 April were orbiting at altitudes below 300 km, while the other 10 satellites were at altitudes of 350 km and 400 km. O/N₂ ratio serves as a proxy for ionization in the upper atmosphere. If we take a look at figures 4 and 5, we can see that the O/N₂ ratio is most enhanced at 400km, followed by 350 km, with minimal variation observed at 300 km around 25 April 2024. This indicates a significant effect of thermospheric expansion at altitudes above 300 km, leading to the uplift of the F layer and increased density at higher altitudes (Tsaouri, 2022).

EUV radiation is a primary driver of thermospheric heating, which in turn causes atmospheric expansion. This expansion increases the density of the thermosphere at satellite altitudes, leading to higher drag forces. The temporal correlation between the EUV irradiance spike (figure 3b) and the observed increase in decay rates suggests a direct link between these factors.

The solar storm of 10 May 2024 was followed by substantial atmospheric disturbances. This included extreme auroral extensions observed as a result of the storm, with the auroral oval extending to below 30° magnetic latitude (Hayakawa et al., 2024). The precipitating particles in the auroral region and intense heating due to auroral electrojets possibly contributed to ionospheric heating. The resulting sudden and significant increase in thermospheric densities caused the rapid decay of satellites following the storm. However, there is a time lag of over 24 hours between the onset of the storm and the sudden change in the decay rate of 10 satellites. Oliveira & Zesta (2019) reported a delay ranging from 12 to 72 hours for extreme to moderate geomagnetic storms, and the delay observed here aligns

with this range. For 10 of the satellites considered in this study, delays of up to 72 hours are seen in the occurrence of maximum decay. This delay is expected for a moderate storm, suggesting that the geoeffectiveness of the May 2024 storm was lower even though it was a G5 storm.

5 Concluding Remarks

The orbital decay and subsequent reentries of 12 Starlink satellites during and before the extreme geomagnetic storm of 10 May 2024 were examined. While the rapid post-storm increase in decay due to atmospheric disturbances was expected, the unexpected increase in decay rates prior to the storm, around 25 April 2024, proved interesting. It was seen that the EUV flux was significantly enhanced during this period, affecting the thermosphere through various processes. This indicated the important role of elevated space weather conditions prior to the storm which resulted in increased satellite drag. These findings underscore the importance of understanding the complex interactions between solar activity, thermospheric dynamics, and satellite drag, particularly in the context of increased use of the LEO environment for space applications by the global community.

Data Availability Statement

All the data used in this work is publicly available. The TLE data for the satellites considered in this study were obtained from the Space-Track website (<https://www.space-track.org>). EUV flux data from SDO was obtained from LISIRD (<https://lasp.colorado.edu/lisird/>). Data on solar wind and interplanetary magnetic fields were obtained from CDAWEB (<https://cdaweb.gsfc.nasa.gov/>), and the Dst index and auroral indices were sourced from the World Data Center in Kyoto (<https://wdc.kugi.kyoto-u.ac.jp/>).

References

- Akasofu, S. I. (1981). Energy coupling between the solar wind and the magnetosphere. *Space Science Reviews*, *28*, 121–190.
- Baumjohann, W., & Kamide, Y. (1984). Hemispherical joule heating and the ae indices. *Journal of Geophysical Research: Space Physics*, *89*(A1), 383-388. doi: <https://doi.org/10.1029/JA089iA01p00383>
- Billett, D. D., Sartipzadeh, K., Ivarsen, M. F., Iorfida, E., Doornbos, E., Kalafatoglu Eyiguler, E. C., ... McWilliams, K. A. (2024). The 2022 starlink geomagnetic storms: Global thermospheric response to a high-latitude ionospheric driver. *Space Weather*, *22*(2), e2023SW003748. doi: <https://doi.org/10.1029/2023SW003748>
- Burton, R. K., McPherron, R., & Russell, C. (1975). An empirical relationship between interplanetary conditions and dst. *Journal of geophysical research*, *80*(31), 4204–4214.
- Chun, F. K., Knipp, D. J., McHarg, M. G., Lacey, J. R., Lu, G., & Emery, B. A. (2002). Joule heating patterns as a function of polar cap index. *Journal of Geophysical Research: Space Physics*, *107*(A7), SIA 8-1-SIA 8-9. doi: <https://doi.org/10.1029/2001JA000246>
- Doornbos, E., & Klinkrad, H. (2006). Modelling of space weather effects on satellite drag. *Advances in Space Research*, *37*(6), 1229-1239. (Space weather prediction: Applications and validation) doi: <https://doi.org/10.1016/j.asr.2005.04.097>
- Emmert, J. T., Drob, D. P., Picone, J. M., Siskind, D. E., Jones Jr., M., Mlynczak, M. G., ... Yuan, T. (2021). Nrlmsis 2.0: A whole-atmosphere empirical model of temperature and neutral species densities. *Earth and Space Science*, *8*(3), e2020EA001321. doi: <https://doi.org/10.1029/2020EA001321>
- España Fontcuberta, A., Ghosh, A., Chatterjee, S., Mitra, D., & Nandy, D. (2023). Forecasting solar cycle 25 with physical model-validated recurrent neural networks. *Solar Physics*, *298*(1), 8.

- Forbes, J. M., Lu, G., Bruinsma, S., Nerem, S., & Zhang, X. (2005). Thermosphere density variations due to the 15–24 april 2002 solar events from champ/star accelerometer measurements. *Journal of Geophysical Research: Space Physics*, *110*(A12). doi: <https://doi.org/10.1029/2004JA010856>
- Hayakawa, H., Ebihara, Y., Mishev, A., Koldobskiy, S., Kusano, K., Bechet, S., . . . Miyoshi, Y. (2024). *The solar and geomagnetic storms in may 2024: A flash data report*. Retrieved from <https://arxiv.org/abs/2407.07665>
- Huang, Y., Richmond, A. D., Deng, Y., & Roble, R. (2012). Height distribution of joule heating and its influence on the thermosphere. *Journal of Geophysical Research: Space Physics*, *117*(A8). doi: <https://doi.org/10.1029/2012JA017885>
- Karan, D. K., Martinis, C. R., Daniell, R. E., Eastes, R. W., Wang, W., McClintock, W. E., . . . England, S. (2024). Gold observations of the merging of the southern crest of the equatorial ionization anomaly and aurora during the 10 and 11 may 2024 mother’s day super geomagnetic storm. *Geophysical Research Letters*, *51*(15), e2024GL110632.
- King, J. H., & Papitashvili, N. E. (2020). *Omni 1-min data set*. NASA Space Physics Data Facility.
- Kwak, Y.-S., Kim, J.-H., Kim, S., Miyashita, Y., Yang, T., Park, S.-H., . . . others (2024). Observational overview of the may 2024 g5-level geomagnetic storm: From solar eruptions to terrestrial consequences. *Journal of Astronomy and Space Sciences*, *41*(3), 171–194.
- Lazzús, J., & Salfate, I. (2024). Report on the effects of the may 2024 mother’s day geomagnetic storm observed from chile. *Journal of Atmospheric and Solar-Terrestrial Physics*, *261*, 106304.
- Liu, H., Lühr, H., & Watanabe, S. (2007). Climatology of the equatorial thermospheric mass density anomaly. *Journal of Geophysical Research: Space Physics*, *112*(A5). doi: <https://doi.org/10.1029/2006JA012199>
- Lu, G., Richmond, A. D., Lühr, H., & Paxton, L. (2016). High-latitude energy input and its impact on the thermosphere. *Journal of Geophysical Research: Space Physics*, *121*(7), 7108–7124. doi: <https://doi.org/10.1002/2015JA022294>
- Mavromichalaki, H., Papailiou, M.-C., Livada, M., Gerontidou, M., Paschalis, P., Stassinakis, A., . . . others (2024). Unusual forrush decreases and geomagnetic storms on 24 march, 2024 and 11 may, 2024. *Atmosphere*, *15*(9), 1033.
- O’Brien, T. P., & McPherron, R. L. (2000). An empirical phase space analysis of ring current dynamics: Solar wind control of injection and decay. *Journal of Geophysical Research: Space Physics*, *105*(A4), 7707–7719.
- Oigawa, T., Shinagawa, H., & Taguchi, S. (2021). Time-dependent responses of the neutral mass density to fixed magnetospheric energy inputs into the cusp region in the thermosphere during a period of large imf b_r : a high-resolution two-dimensional local modeling. *Earth Planets Space*, *73*(201). doi: <https://doi.org/10.1186/s40623-021-01535-9>
- Oliveira, D. M., & Zesta, E. (2019). Satellite orbital drag during magnetic storms. *Space Weather*, *17*(11), 1510–1533. doi: <https://doi.org/10.1029/2019SW002287>
- Oliveira, D. M., Zesta, E., Hayakawa, H., & Bhaskar, A. (2020). Estimating satellite orbital drag during historical magnetic superstorms. *Space Weather*, *18*(11), e2020SW002472. doi: <https://doi.org/10.1029/2020SW002472>
- Parker, W. E., & Linares, R. (2024). Satellite drag analysis during the may 2024 gannon geomagnetic storm. *Journal of Spacecraft and Rockets*, 1–5.
- Pierrard, V., Winant, A., Botek, E., & de Bonhome, M. P. (2024). The mother’s day solar storm of 11 may 2024 and its effect on earth’s radiation belts.
- Poudel, P., Simkhada, S., Adhikari, B., Sharma, D., & Nakarmi, J. J. (2019). Variation of solar wind parameters along with the understanding of energy dynamics within the magnetospheric system during geomagnetic disturbances. *Earth and Space Science*, *6*(2), 276–293.
- Sutton, E. K., Forbes, J. M., & Knipp, D. J. (2009). Rapid response of the thermosphere to variations in joule heating. *Journal of Geophysical Research: Space Physics*, *114*(A4). doi: <https://doi.org/10.1029/2008JA013667>

- Thampi, S. V., Venugopal, I., & Bhaskar, A. T. (2024). Super-fountain effect: Unleashing the role of electric fields during the extreme geomagnetic storm on may 10-11, 2024. *Authorea Preprints*. doi: <https://doi.org/10.22541/essoar.172434426.60233888/v1>
- Tsagouri, I. (2022). Space weather effects on the earth's upper atmosphere: Short report on ionospheric storm effects at middle latitudes. *Atmosphere*, *13*(2). doi: 10.3390/atmos13020346
- Vallado, D., & Cefola, P. (2012, 01). Two-line element sets - practice and use. *Proceedings of the International Astronautical Congress, IAC*, *7*, 5812-5825.
- Vichare, G., Alex, S., & Lakhina, G. (2005). Some characteristics of intense geomagnetic storms and their energy budget. *Journal of Geophysical Research: Space Physics*, *110*(A3).
- Vichare, G., Bhaskar, A., Rawat, R., Yadav, V., Mishra, W., Angchuk, D., & Singh, A. K. (2024). Low-latitude auroras: Insights from 23 april 2023 solar storm. *arXiv preprint arXiv:2405.08821*.
- Vourlidas, A., & Bruinsma, S. (2018). Euv irradiance inputs to thermospheric density models: Open issues and path forward. *Space Weather*, *16*(1), 5-15. doi: <https://doi.org/10.1002/2017SW001725>
- Wang, C., Chao, J., & Lin, C.-H. (2003). Influence of the solar wind dynamic pressure on the decay and injection of the ring current. *Journal of Geophysical Research: Space Physics*, *108*(A9).
- Woods, T., Eparvier, F., & Hock, R. e. a. (2012). Extreme ultraviolet variability experiment (eve) on the solar dynamics observatory (sdo): Overview of science objectives, instrument design, data products, and model developments. *Sol Phys*, *275*, 115–143. doi: <https://doi.org/10.1007/s11207-009-9487-6>
- Yokoyama, N., & Kamide, Y. (1997). Statistical nature of geomagnetic storms. *Journal of Geophysical Research: Space Physics*, *102*(A7), 14215–14222.
- Yu, T., Wang, W., Ren, Z., Cai, X., & He, M. (2023). Vertical variations in thermospheric o/n2 and the relationship between o and n2 perturbations during a geomagnetic storm. *Earth and Space Science*, *10*(10), e2023EA002988. doi: <https://doi.org/10.1029/2023EA002988>
- Zesta, E., & Oliveira, D. M. (2019). Thermospheric heating and cooling times during geomagnetic storms, including extreme events. *Geophysical Research Letters*, *46*(22), 12739–12746.